Available online at www.sciencedirect.com

ScienceDirect

Geochimica et Cosmochimica Acta 218 (2017) 58–72

Geochimica et Cosmochimica Acta

www.elsevier.com/locate/gca

Origin of heavy Fe isotope compositions in high-silica igneous rocks: A rhyolite perspective

De-Hong Du, Xiao-Lei Wang *, Tao Yang, Xin Chen, Jun-Yong Li, Weiqiang Li *

State Key Laboratory for Mineral Deposits Research, School of Earth Sciences and Engineering, Nanjing University, Nanjing 210046, China

Received 4 March 2017; accepted in revised form 2 September 2017; Available online 9 September 2017

Abstract

The origin of heavy Fe isotope compositions in high-silica (>70 wt% SiO_2) igneous rocks remains a highly controversial topic. Considering that fluid exsolution in eruptive rocks is more straight-forward to constrain than in plutonic rocks, this study addresses the problem of Fe isotope fractionation in high-silica igneous rocks by measuring Fe isotope compositions of representative rhyolitic samples from the Neoproterozoic volcanic-sedimentary basins in southern China and the Triassic Tu Le Basin in northern Vietnam. The samples show remarkably varied $\delta^{56}Fe_{IRMM014}$ values ranging from $0.05 \pm 0.05‰$ to $0.55 \pm 0.05‰$, which is among the highest values reported from felsic rocks. The extensional tectonic setting and short melt residence time in magma chambers for the studied rhyolites rule out Soret diffusion and thermal migration processes as causes of the high $\delta^{56}Fe$ values. Effects of volcanic degassing and fluid exsolution on bulk rock $\delta^{56}Fe$ values for the rhyolites are also assessed using bulk rock geochemical indicators and Rayleigh fractionation models, and these processes are found to be insufficient to produce resolvable changes in Fe isotope compositions of the residual melt. The most probable mechanism accounting for heavy Fe isotope compositions in the high-silica rhyolites is narrowed down to fractional crystallization processes in the magma before rhyolite eruption. Removal of isotopically light Fe-bearing minerals (i.e. ulvöspinel-rich titanomagnetite, ilmenite and biotite) is proposed as the main cause of Fe isotope variation in silicic melts during magmatic evolution. This study implies that crystal fractionation is the dominant mechanism that controls Fe isotope fractionation in eruptive rocks and Fe isotopes could be used to study magmatic differentiation of high-silica magmas.

Keywords: Fe isotopes; High-SiO_2 rhyolites; Fractional crystallization; Isotopic fractionation; Mechanism

1. INTRODUCTION

Iron is a major polyvalent metal that plays a key role in a variety of magmatic and mineralizing processes on Earth. The usefulness of Fe isotopes as a potential tracer for these processes has been studied extensively. Most of crustal igneous rocks have limited variation in Fe isotope composition ($0.09 \pm 0.08‰$ in $^{56}Fe/^{54}Fe$ relative to IRMM-014; Heimann et al., 2008; Teng et al., 2013), but there is a remarkable enrichment in heavy Fe isotopes (up to 0.5‰ increase in $^{56}Fe/^{54}Fe$ ratios relative to average crustal igneous rocks) in high-silica (>70 wt% SiO_2) igneous rocks (Poitrasson and Freydier, 2005; Heimann et al., 2008; Schuessler et al., 2009; Telus et al., 2012; Zambardi et al., 2014; Foden et al., 2015; Gajos et al., 2016; Xia et al., 2017). Four possible mechanisms have been proposed to explain the heavy Fe isotopic signatures in high-SiO_2 rocks: (1) fractional crystallization of minerals that are enriched in light Fe isotopes (Schuessler et al., 2009; Sossi et al., 2012; Foden et al., 2015; Xia et al., 2017); (2) exsolution of fluids with isotopically light Fe isotopes (Poitrasson and Freydier, 2005; Heimann et al., 2008; Telus et al., 2012); (3) Soret

* Corresponding authors.
E-mail addresses: wxl@nju.edu.cn (X.-L. Wang), liweiqiang@nju.edu.cn (W. Li).

http://dx.doi.org/10.1016/j.gca.2017.09.014
0016-7037/

effect and thermal migration during magmatic processes (Huang et al., 2009; Lundstrom, 2009; Richter et al., 2009; Zambardi et al., 2014; Gajos et al., 2016); and (4) partial melting (Telus et al., 2012; Xu et al., 2017). Elucidating the exact origin of heavy Fe isotope compositions bears on interpretation of magmatic evolution of high-SiO_2 igneous rocks using Fe isotopes, yet the origin of high δ^{56}Fe signatures in high-SiO_2 igneous rocks remains a hot topic of debate over the past few years.

Previous studies on heavy Fe isotope signatures of high-SiO_2 rocks generally concentrated on plutonic rocks. Relative to eruptive rocks, plutonic rocks commonly record protracted periods from magma intrusion to solidification and complete waning of volatile exsolution. The behaviors of volatiles/fluids during such long periods are commonly rather complicated to evaluate for a pluton. Because volatiles could build up within the upper part of a solidifying magma chamber, and the fluid pathway of devolatilization in a degassing pluton cannot be homogeneous, there could be remarkable heterogeneity in actual fluid/rock ratios within an intrusive rock body. Furthermore, exsolved volatiles can be present in forms of vapor and brine (Driesner and Heinrich, 2007; Zajacz et al., 2008; Wawryk and Foden, 2015). All of these increase the complexity in interpretation of Fe isotope signatures of high-SiO_2 plutonic rocks from a fluid exsolution perspective. In contrast, fluid exsolution is more straight forward to constrain for eruptive rocks (such as rhyolite and tuff), because available experimental studies have suggested that eruptive rocks will lose most of their primary dissolved volatiles upon eruption in response to pressure unloading (Williams-Jones and Heinrich, 2005; Baker and Alletti, 2012; Sigurdsson et al., 2015). Therefore, eruptive rocks seem to be a better candidate for evaluating the proposed mechanisms for Fe isotope fractionation in high-SiO_2 igneous rocks as complexities in fluid exsolution are greatly reduced. However, only limited Fe isotopic data have been reported for high-SiO_2 eruptive rocks and none of the previous Fe isotope fractionation studies were dedicated to rhyolites (e.g. Heimann et al., 2008; Schuessler et al., 2009; Zambardi et al., 2014).

In this study, we investigated the Fe isotope systematics of representative high-SiO_2 rhyolitic rocks from the Neoproterozoic volcanic-sedimentary basins in southern China and the Triassic Tu Le Basin in northern Vietnam. The roles of volcanic degassing and fractional crystallization on iron isotope fractionations of the rocks are quantitatively evaluated through geochemical modeling. Evidence from rhyolite elucidates the relative contributions of the two processes on Fe isotope variability, and provides new insights into how Fe isotopes can be used to understand magmatic differentiation of high-Si rocks.

2. GEOLOGICAL BACKGROUND AND SAMPLES

The South China Block (SCB) consists of the Yangtze and the Cathaysia blocks. It is separated from the North China Craton by the Qinling-Dabie Orogen to the north, from the Songpan-Ganzi Block by the Longmenshan Fault to the west, and from the Indochina Block to the southwest by the Song Ma suture (Fig. 1). Neoproterozoic rift/extension systems were extensively developed throughout the SCB after amalgamation of the Yangtze and the Cathaysia blocks at ca. 860–820 Ma (Wang et al., 2014), producing volcanic-sedimentary rocks that unconformably overly the Neoproterozoic folded basements and orogen-related magmatic complexes (Wang and Li, 2003). Bimodal magmatism, OIB-like mafic rocks and high-silica volcanic rocks are common within the Neoproterozoic rift/extension systems (Li et al., 2002, 2008; Wang et al., 2008, 2012). Two suites of volcanic-sedimentary sequences in the rift/extension systems were selected for this study: one is the Shangshu Formation that is located on the southeastern margin of the Yangtze Block (Fig. 1), and the other is the Suxiong Formation that is located on the western margin of the western Yangtze Block (Fig. 1). The felsic rocks of these two suites show geochemical characteristics similar to A-type granites (Li et al., 2002, 2008; Wang et al., 2012). Published zircon U-Pb dating results suggest that both sets of rocks formed at ca. 800 Ma (Li et al., 2002, 2008; Wang et al., 2012). The Shangshu felsic rocks were formed by reworking of early Neoproterozoic juvenile arc crustal materials (Wang et al., 2012). Most of the studied rocks are rhyolite, and a few samples of dacite and trachydacite were also selected for Fe isotope analysis (Fig. 2). Eight samples were selected from the Shangshu Formation and they show porphyritic texture with phenocrysts of K-feldspar and quartz, with minor plagioclase and biotite. The groundmass is composed of feldspar and quartz with accessory ilmenite and zircon (Appendix B Fig. S1). The Suxiong felsic rocks were derived from partial melting of Mesoproterozoic crustal materials (Li et al., 2002, 2005). Porphyritic texture is common in the Suxiong samples, which contain phenocrysts of K-feldspar, plagioclase and quartz. The groundmass is composed of feldspar and quartz, with accessory ilmenite, magnetite and zircon (Appendix B Fig. S1).

In addition to the above two volcanic-sedimentary suites that are related to Neoproterozoic extension in the SCB, a third suite of high-silica volcanic rocks was selected from the Triassic Tu Le Basin of northern Vietnam (Fig. 1). As shown in Fig. 1, the Tu Le Basin extends parallel to the adjacent Ailaoshan-Red River (ASRR) shear zone and the Song Ma suture in northern Vietnam. The basin is composed of felsic volcanic rocks and minor basalts (Lan et al., 2000; Tran et al., 2015). It is suggested to be originally a part of the southern Emeishan Large Igneous Province, but was later extruded to present position by collision between Eurasia and India and strike-slip movement along the ASRR shear zone (e.g. Tapponnier et al., 1990; Leloup et al., 1995; Chung et al., 1997; Tran et al., 2015). The felsic rocks also share geochemical characters of typical A-type granites (Tran et al., 2015). Nine high-silica rhyolite samples (Fig. 2; sample names starting as 15VN-) from the Tu Le Basin were selected for iron isotope analyses and they also show porphyritic texture with phenocrysts being K-feldspar, plagioclase and quartz and the groundmass composed of quartz, feldspar and rare biotite. The accessory minerals include ilmenite, magnetite and zircon (Appendix B Fig. S1).

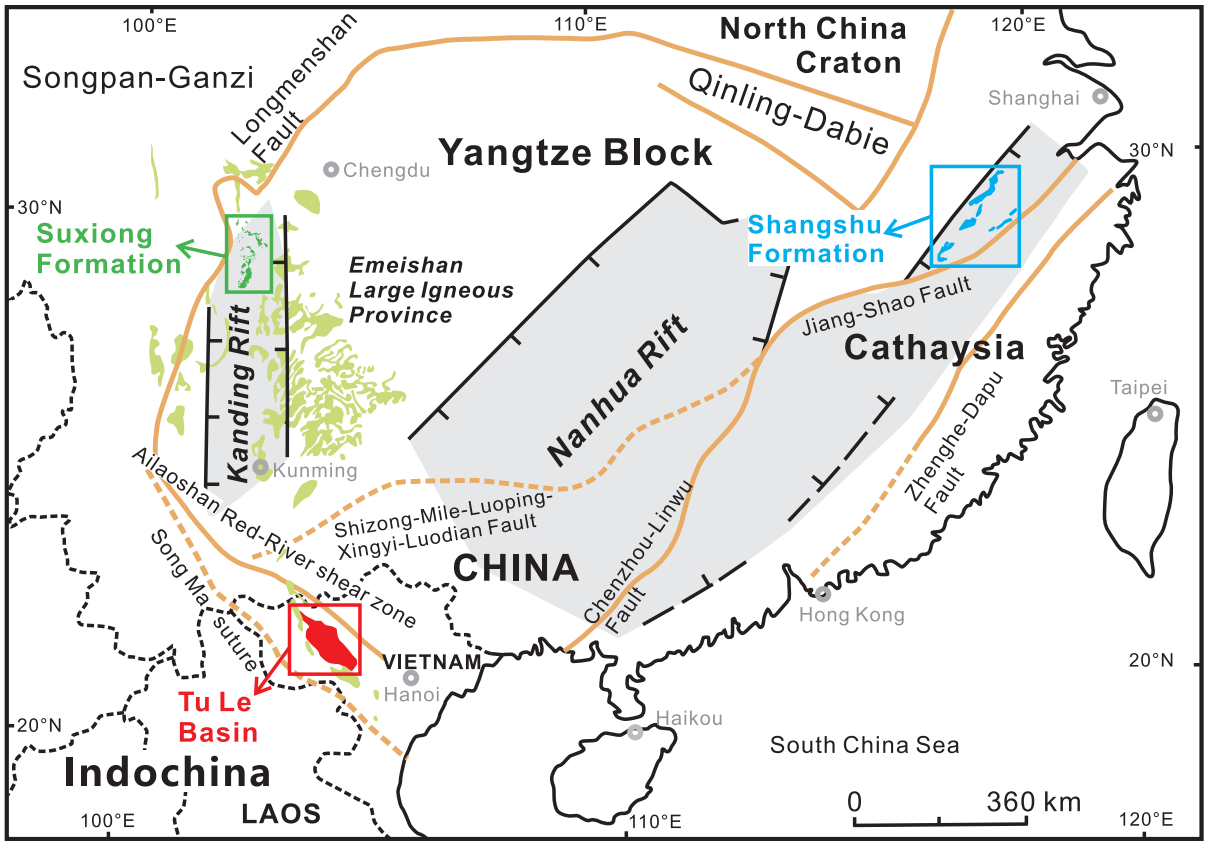

Fig. 1. Geological map of south China and north Vietnam showing the locations of Suxiong and Shangshu formations, and Tu Le Basin (modified after Chung et al., 1997; Wang and Li, 2003; Zhao and Cawood, 2012).

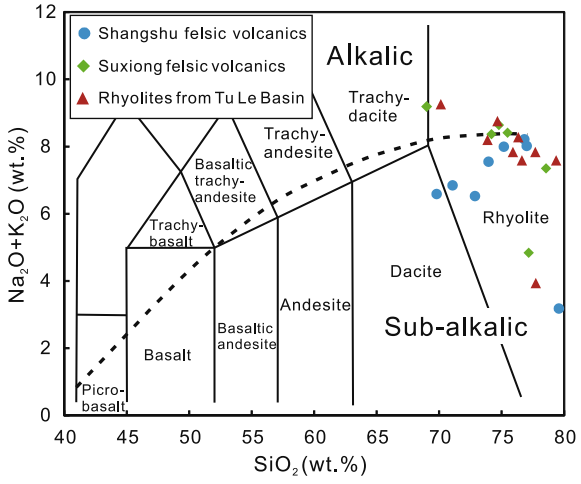

Fig. 2. Diagram of total alkalis versus SiO_2 for the ryholitic rocks.

3. METHODS

3.1. Major- and trace-element analyses

Major-element compositions of the samples from the Suxiong Formation and the Tu Le Basin were analyzed using an X-ray fluorescence spectrometer (XRF) at ALS Chemex (Guangzhou). Analytical precision (RSD) is 1–3% for elements with content above 1 wt% and is better than 5% for elements with contents below 1 wt%. Trace-element concentrations were determined by inductively coupled plasma-mass spectrometry (ICP-MS) at Nanjing FocuMS Technology Co. Ltd., with analytical precision better than 5% for trace elements with concentrations >50 ppm and better than 10% for trace elements with concentrations <50 ppm. The results are shown in the Table S1 of the supplementary Appendix A.

3.2. Fe isotope analysis

Sample preparation was undertaken at State Key Laboratory for Mineral Deposit Research, Nanjing University, where all chemical procedures were performed in a clean room with laminar flow hoods and HEPA filtered air. Deionized (18.2 MΩ) water, Teflon-coated hot plates, Teflon beakers, double distilled reagents were used throughout the experiments; other labwares such as centrifuge tubes and pipette tips were soaked in 6 M HCl overnight, rinsed using deionized water and dried before usage. Approximately 10 to 150 mg bulk-rock powder for each sample was digested in a 2:1:1 mixture of concentrated HCl-HNO_3-HF in 7 mL Teflon beakers on hot-plate at ~130 °C for 2 days. After evaporation, the samples were completely dissolved in a 3:1 mixture of concentrated HCl-HNO_3 and dried again. The fully dissolved samples

were converted to chloride form by repeated redissolution in 1 mL concentrated HCl and subsequent evaporation to dryness. The samples were finally dissolved in 5 mL 7 M HCl and stored in a Teflon beaker as sample stock solution. Based on measured Fe concentrations, an aliquot of the sample stock solution that contained 100 μg Fe was extracted and evaporated to dryness and then dissolved in 100 μL 7 M HCl for chemical purification.

Iron was separated from matrix elements by anion exchange chromatography using 0.2 mL Bio-Rad AG MP-1 resin in a custom-made shrinkable Teflon column. Before anion exchange, the resin was cleaned with 1 mL 2% (volume ratio) HNO_3 and 1 mL Milli-Q H_2O, then conditioned with 2 mL 7 M HCl. After loading 100 μL sample solution in 7 M HCl onto the resin, the matrix elements were eluted off the column using 3 mL of 7 M HCl in 0.5 mL increments. Iron was subsequently eluted from the resin using 3 mL of 2% HNO_3. The Fe cut was evaporated to dryness, redissolved in 100 μL sample in 7 M HCl, and was purified for a second time by repeating the anion exchange procedure as described above. Purified Fe was dried and treated with three drops of 30% H_2O_2 and 2 mL concentrated HNO_3 to decompose organic matters. Then Fe was dissolved in 4 mL 2% HNO_3 and ready for Fe isotope analysis.

Iron isotope ratios were measured using a Thermo Fisher Scientific Neptune Plus MC-ICP-MS at State Key Laboratory for Mineral Deposit Research, Nanjing University. The instrument was running at "wet-plasma" mode using a 100 μL/min self-aspirating nebulizer tip and a glass spray chamber. Molecular interferences of $^{40}Ar^{14}N^+$ and $^{40}Ar^{16}O^+$ on $^{54}Fe^+$ and $^{56}Fe^+$ were fully resolved using high mass resolution setting of the instrument at the low mass shoulders. Isobaric interference of $^{54}Cr^+$ on $^{54}Fe^+$ was monitored by simultaneous measurement of $^{53}Cr^+$ signals and was corrected offline. Instrument sensitivity was 4–6 V/ppm on $^{56}Fe^+$ with the instrument setting. A standard-sample-standard bracketing routine was applied for Fe isotope ratio measurement, and samples were diluted to 2 ± 0.2 ppm to match the concentration of an in-house standard that was constant at 2.0 ppm. A 40 s on-peak acid blank was measured before each analysis. Each Fe isotope ratio measurement consisted of fifty 4-s integrations, and the typical internal precision (2 standard error or 2SE) was better than ± 0.03‰ for $^{56}Fe/^{54}Fe$ and ± 0.05‰ for $^{57}Fe/^{54}Fe$. The long-term external reproducibility (2 standard deviation or 2SD) of Fe isotope analysis is better than ±0.06‰ in $^{56}Fe/^{54}Fe$ and ±0.16‰ in $^{57}Fe/^{54}Fe$ over six months, based on repeat analysis of multiple Fe isotope standard solutions against in-house stock solutions (Table 1).

Iron isotope compositions are reported as $\delta^{56}Fe$ relative to the international standard of IRMM-014:

$$\delta^{56}Fe_{sample} = [(^{56}Fe/^{54}Fe)_{sample}/(^{56}Fe/^{54}Fe)_{IRMM-014} - 1] \times 1000[‰]$$

Accuracy of Fe isotope measurements was confirmed by repeated measurements of reference samples and geostandards that were treated as unknowns with the rhyolite samples. $\delta^{56}Fe$ of two ultrapure Fe solutions from University of Wisconsin-Madison, J-M Fe and HPS Fe, are 0.37 ± 0.06‰ ($n = 10$, 2SD) and 0.58 ± 0.06‰ ($n = 7$, 2SD), respectively, which are in excellent agreements with the recommended values (Beard et al., 2003; Heimann et al., 2008). In addition, the measured Fe isotope compositions of the international whole-rock standards, DNC-1a ($\delta^{56}Fe = 0.02 \pm 0.06$‰; $n = 3$, 2SD), BCR-2 ($\delta^{56}Fe = 0.11 \pm 0.08$‰; $n = 9$, 2SD), BHVO-2 ($\delta^{56}Fe = 0.13 \pm 0.05$‰; $n = 9$, 2SD), BIR-1a ($\delta^{56}Fe = 0.08 \pm 0.06$‰; $n = 3$, 2SD) and DTS-2b ($\delta^{56}Fe = 0.06 \pm 0.08$‰; $n = 3$, 2 SD), are all consistent with the recommended values (Craddock and Dauphas, 2011; He et al., 2015) within analytical uncertainties (Table 1). For igneous rocks investigated in this study, each sample was measured at least three times and analytical uncertainties of Fe isotope ratios were given as 2SD.

4. RESULTS

The $\delta^{56}Fe$ values for the rhyolitic rocks from the three volcanic basins show a large variation from 0.05 ± 0.05‰ to 0.55 ± 0.05‰ (Table 1). Among them, the samples from the Shangshu Formation have $\delta^{56}Fe$ values ranging from 0.19 ± 0.02‰ to 0.37 ± 0.01‰, and those from the Tu Le Basin have $\delta^{56}Fe$ values varying from 0.05 ± 0.03‰ to 0.42 ± 0.05‰ (Fig. 3). These values are consistent with the published data range for igneous rocks (0–0.4‰; Poitrasson and Freydier, 2005; Heimann et al., 2008; Schuessler et al., 2009; Telus et al., 2012; Zambardi et al., 2014; Foden et al., 2015). Notably, samples of the Suxiong Formation have $\delta^{56}Fe$ values varying from 0.13 ± 0.01‰ to 0.55 ± 0.05‰, which show a similar variability (about 0.4 ‰) but give values among the heaviest Fe isotope compositions of igneous rocks yet reported. In addition, $\delta^{56}Fe$ values of these rhyolitic rocks show negative correlation with indexes of igneous differentiation including $Fe_2O_3^t$ (total iron) and MgO contents, as well as Eu/Eu^* ratios, suggesting loss of a low-$\delta^{56}Fe$ components during magmatic evolution (Fig. 3). In contrast, $\delta^{56}Fe$ values of the rocks are poorly correlated with SiO_2 contents (Fig. 3), which may reflect the insensitivity of SiO_2 contents to the differentiation of high-silica melts (Heimann et al., 2008).

5. DISCUSSION

5.1. The role of Soret diffusion and thermal migration in iron isotope fractionation

Previous experimental studies suggested that temperature gradients imposed on silicate melt can lead to Fe isotope fractionation, with enrichment of heavy and light isotopes occurring at the cold and hot ends of the melt, respectively (Huang et al., 2009; Richter et al., 2009). These experiments can be divided into two categories based on experimental conditions and behaviors of major elements: (1) Soret diffusion in completely molten melts, with the hot end enriched in SiO_2 and Na_2O and the cold end enriched in CaO, Fe_2O_3 and MgO (Richter et al., 2009); and (2) thermal migration under partially molten condi-

Table 1
Iron isotope and major element compositions of reference materials and rhyolitic samples in this study.

Rock type	Sample	δ^{56}Fe (‰)	δ^{57}Fe (‰)	Major elment composition (wt%)										
		±2SD	±2SD	SiO_2	TiO_2	Al_2O_3	Fe_2O_3	MnO	MgO	CaO	Na_2O	K_2O	P_2O_5	LOI
Reference materials														
	J-M Fe	0.37 ± 0.06	0.54 ± 0.13											
	HPS Fe	0.58 ± 0.06	0.84 ± 0.11											
	DNC-1a	0.02 ± 0.06	0.04 ± 0.03											
	BCR-2	0.11 ± 0.08	0.18 ± 0.12											
	BHVO-2	0.13 ± 0.05	0.25 ± 0.13											
	BIR-1a	0.08 ± 0.06	0.15 ± 0.11											
	DTS-2b	0.06 ± 0.08	0.08 ± 0.14											
Shangshu Formation, S China														
Rhyolite	10SS-2-1	0.19 ± 0.02	0.32 ± 0.06	72.86	0.21	12.72	3.01	0.06	0.41	0.90	2.56	3.97	0.07	1.33
Rhyolite	10SS-3-2	0.26 ± 0.05	0.35 ± 0.12	75.17	0.20	12.44	2.22	0.03	0.11	0.61	3.69	4.31	0.03	1.03
Rhyolite	10SS-4-2	0.19 ± 0.06	0.30 ± 0.14	71.07	0.39	14.54	2.85	0.04	0.65	1.27	2.93	3.92	0.17	1.74
Dacite	10SS-5-1	0.22 ± 0.05	0.34 ± 0.10	69.80	0.44	14.54	3.27	0.05	0.87	1.78	3.62	2.97	0.17	2.22
Rhyolite	10SS-8-1	0.32 ± 0.01	0.50 ± 0.05	77.00	0.10	12.34	1.04	0.01	0.15	0.44	3.42	4.60	0.01	0.82
Rhyolite	10SS-12-1	0.37 ± 0.01	0.53 ± 0.03	76.81	0.05	12.13	0.83	0.01	0.08	0.06	3.48	4.74	0.01	0.58
Rhyolite	10SS-14-1	0.21 ± 0.04	0.31 ± 0.06	73.95	0.21	13.41	2.00	0.02	0.31	0.81	3.35	4.20	0.04	1.16
Rhyolite	09WN-1-1	0.27 ± 0.06	0.35 ± 0.18	79.57	0.54	12.05	1.82	0.07	0.19	0.06	0.46	2.72	0.03	2.23
Suxiong Formation, S China														
Rhyolite	15SX-1-1	0.3 ± 0.03	0.46 ± 0.05	74.19	0.36	12.66	2.51	0.04	0.42	0.32	3.17	5.20	0.09	1.18
Rhyolite	15SX-2	0.39 ± 0.01	0.58 ± 0.13	74.78	0.19	12.50	1.82	0.03	0.11	0.31	3.35	5.29	0.01	0.91
Rhyolite	15SX-3-2	0.55 ± 0.05	0.81 ± 0.06	75.48	0.13	11.77	1.28	0.01	0.17	0.01	0.16	8.25	0.01	1.65
Rhyolite	15SX-10-1	0.46 ± 0.03	0.70 ± 0.03	77.16	0.11	11.63	1.19	0.09	0.06	1.46	2.64	2.20	0.02	2.52
Rhyolite	15SX-10-2	0.52 ± 0.05	0.76 ± 0.15	81.98	0.08	10.39	0.78	0.02	0.05	0.29	2.61	1.93	0.02	1.36
Rhyolite	15SX-11-1	0.23 ± 0.05	0.38 ± 0.16	78.56	0.16	11.33	1.30	0.02	0.10	0.14	2.06	5.29	0.02	0.89
Trachydacite	15SX-12-1	0.13 ± 0.01	0.19 ± 0.07	69.00	0.52	14.20	4.07	0.07	0.63	0.34	4.58	4.61	0.17	0.90
Tu Lu Basin, N Vietnam														
Rhyolite	15VN-19-1	0.18 ± 0.09	0.28 ± 0.19	76.62	0.24	10.77	2.80	0.04	0.34	0.06	1.97	5.62	0.01	0.56
Rhyolite	15VN-19-2	0.12 ± 0.02	0.21 ± 0.03	73.87	0.35	12.09	2.62	0.04	0.64	0.15	4.06	4.14	0.04	0.70
Rhyolite	15VN-20-1	0.32 ± 0.06	0.54 ± 0.15	75.90	0.27	11.46	2.91	0.04	0.20	0.04	2.83	5.01	0.01	0.64
Rhyolite	15VN-20-3	0.22 ± 0.03	0.33 ± 0.09	77.70	0.27	11.36	2.02	0.04	0.18	0.05	2.92	4.92	0.01	0.55
Rhyolite	15VN-21-2	0.16 ± 0.02	0.23 ± 0.04	70.13	0.56	13.44	4.31	0.12	0.35	0.71	4.47	4.79	0.11	0.56
Rhyolite	15VN-22-1	0.11 ± 0.04	0.20 ± 0.10	79.36	0.18	9.65	1.02	0.01	0.87	0.05	0.13	7.46	0.02	1.08
Rhyolite	15VN-23-1	0.21 ± 0.02	0.30 ± 0.09	77.74	0.33	10.61	3.61	0.12	0.43	0.14	0.64	3.30	0.03	2.82
Rhyolite	15VN-49-1	0.42 ± 0.05	0.62 ± 0.13	76.33	0.22	10.62	2.66	0.04	0.18	0.15	3.06	5.22	0.01	0.56
Rhyolite	15VN-50-1	0.05 ± 0.03	0.10 ± 0.12	74.67	0.33	12.21	3.03	0.14	0.12	0.09	4.16	4.60	0.02	1.07

Note: The major element data of the Shangshu Formation are from Wang et al. (2012).

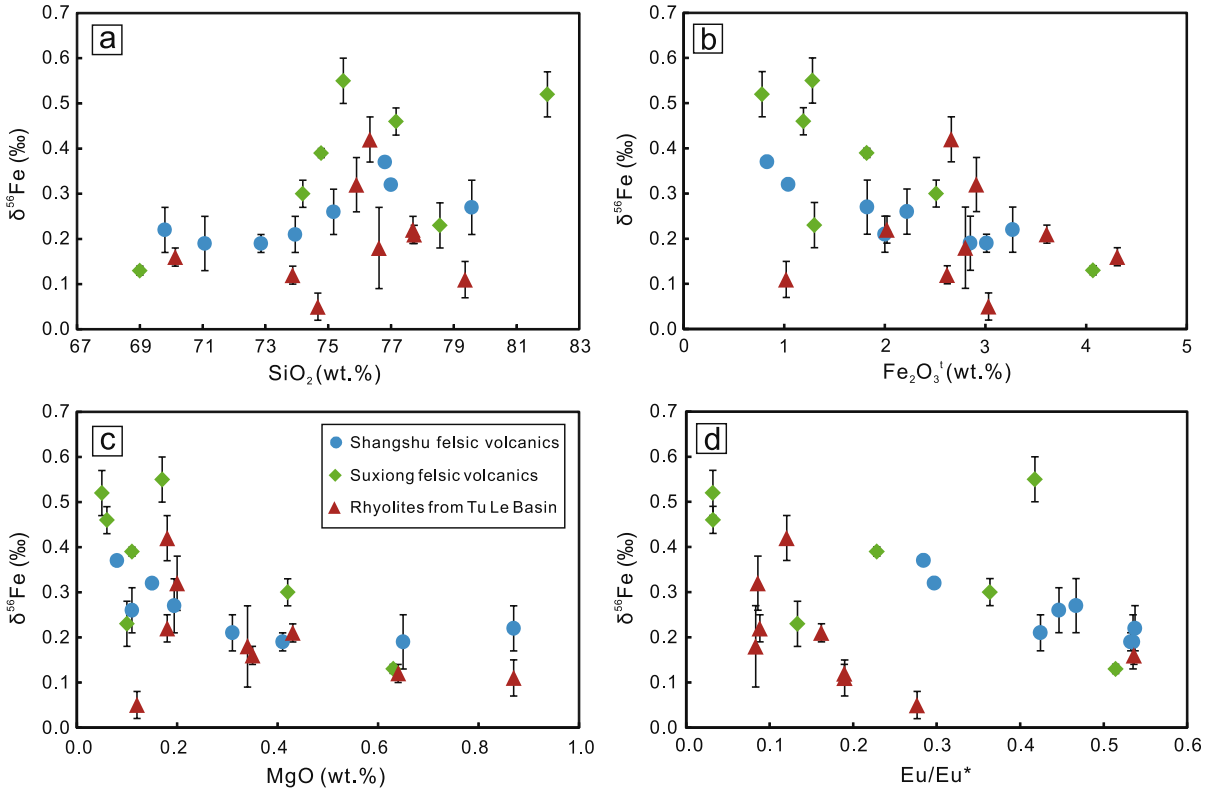

Fig. 3. Iron isotope composition of the rhyolitic rocks as a function of (a) SiO_2, (b) $Fe_2O_3^t$ (total iron content), (c) MgO and (d) Eu/Eu*. Error bar denotes two standard deviations (2SD).

tions, with the cold end enriched in SiO_2 and the hot end enriched in Fe_2O_3 and MgO (Huang et al., 2009). High-silica igneous rocks are expected to be enriched in light iron isotopes according to Soret diffusion (Richter et al., 2009), which is opposite to the observed high δ^{56}Fe as shown in this and previous studies (e.g. Poitrasson and Freydier, 2005; Heimann et al., 2008; Foden et al., 2015). Therefore, Soret diffusion cannot explain the observed heavy Fe isotope compositions for most of high-SiO_2 igneous rocks.

Thermal migration can produce the compositional trends observed in silicic rock series. For example, Gajos et al. (2016) reported a spatial pattern of Fe isotope compositions from the Torres del Paine igneous complex, where δ^{56}Fe values are high in the marginal granites, but lower in the interior granites and the lowest in the mafic base, and this pattern was interpreted as results of thermal migration within the magma chamber. Iron isotope variability in the Cedar Butte volcano was also attributed to a thermal migration process (Zambardi et al., 2014). Lundstrom (2009) suggested that a steady temperature gradient can be produced in a convergent geological setting where the thick volcanic production becomes a barrier to prevent further ascent of magma, inducing top-down compositional zoning from silicic to mafic sequence and heavy to light isotopic trend with increasing depth. This hypothesis has been tested using a multi-isotope approach on selected intrusive rocks and volcanic rocks, but the expected correlations of Mg-Fe, U-Fe and Zn-Fe isotopic fractionations were not observed (Telus et al., 2012; Xia et al., 2017), suggesting that thermal migration is not significant for the investigated rocks. In the case of this study, all rocks investigated were formed in extensional tectonic settings (e.g. Chung et al., 1997; Wang and Li, 2003; Wang et al., 2012) where fractures were developed and the crusts were thinner than in convergent regimes, leading to fast ascent of magma and the bimodal signatures in geochemistry of rocks (Li et al., 2002; Wang et al., 2012; Tran et al., 2015). In this regard, near-steady temperature gradient and migration of iron isotopes were unlikely to have been attained for the rhyolitic rocks of this study.

5.2. Volcanic degassing (fluid exsolution): geochemical and modeling constraints

Silicate melts may contain up to a few weight percent of dissolved volatiles, in which H_2O is the dominant phase, followed by CO_2, SO_2 and HCl, and minor HF, H_2S and CO (Williams-Jones and Heinrich, 2005; Sigurdsson et al., 2015; and references therein). The solubility of volatiles in silicate melts is strongly dependent on pressure (Baker and Alletti, 2012; and references therein). Oversaturation of volatiles can be triggered by magma ascent and associated decompression, which lead to exsolution of volatiles from melt in form of bubbles. When magma reaches the near-surface level of crust, fragmentation occurs and bubbles break up, releasing volatiles into atmosphere (Zhang et al., 2007; Sigurdsson et al., 2015). Both laboratory experiments and observations of natural samples illustrated a

marked capacity of water-rich vapor to transport iron in form of Fe-chloride complexes (Simon et al., 2004; Williams-Jones and Heinrich, 2005; Zajacz et al., 2008; Hill et al., 2010). Furthermore, the negative Fe isotope fractionation factor between Fe-bearing fluids and silicate melts at magmatic temperature (Heimann et al., 2008; also shown in later calculation) indicates that exsolution of Fe-chloride bearing fluid will drive the evolving melt towards heavier Fe isotope compositions. Hence, volatiles exsolved from melt in form of vapor could cause fractionation of Fe isotopes.

Lithium is a fluid-mobile element and its isotopic fractionation is observed during fluid-rock interaction (e.g. Webster et al., 1989; Teng et al., 2006). However, significant Li isotope fractionation is absent in volcanic rocks from the Hekla volcano (Schuessler et al., 2009), implying that the role of volcanic degassing in generating isotopic fractionation can be insignificant. On the other hand, Zr/Hf ratio has been used as an indicator of fluid exsolution in magma because it remains near-chondritic (26–46) during melt-mineral partitioning but decreases significantly (below 26) during fluid-magma interaction, because Zr partitions favorably into the aqueous fluid in F-bearing system over Hf (Bau, 1996; Wilke et al., 2012; Louvel et al., 2014) and F tends to accumulate in differentiated magmas (e.g. Webster and Holloway, 1990). Heimann et al. (2008) reported that igneous samples with sub-chondritic Zr/Hf ratios have higher δ^{56}Fe values, and argued that exsolution of fluids with isotopically light Fe produced the heavy iron isotope compositions in residual high-silica melts for their samples. However, the extent of fluid exsolution was not quantified in the study of Heimann et al. (2008) and it is unclear whether other mechanisms have also contributed along with the decreasing of Zr/Hf ratios.

Different from the study of Heimann et al. (2008), the rhyolitic rocks investigated in this study have near-chondritic Zr/Hf ratios (28–43) except for two samples (10SS-8-1 and 10SS-12-1) from the Shangshu Formation (Fig. 4a). It should be noted that the Zr/Hf ratios of the Shangshu samples are negatively correlated with indicators of igneous differentiation, such as TiO_2 (Fig. 4b) and other indexes (e.g. $Fe_2O_3^t$, MnO, Th, Zn/Fe; Appendix B Fig. S2), indicating the two low Zr/Hf samples were produced by continuous magma differentiation (e.g. zircon crystallization) rather than fluid-magma interaction as the partition coefficient of Zr between zircon and melt is higher than Hf in most cases (Linnen and Keppler, 2002; Bea et al., 2006). In addition, the rhyolite samples with near-chondritic Zr/Hf ratios and the two low Zr/Hf samples from the Shangshu Formation still show high δ^{56}Fe signatures (Fig. 4a), indicating that volcanic degassing had limited effects on Fe isotope fractionation for the rhyolites. Other geochemical indicators for fluid-melt/rock interaction, such as "tetrad effects" of rare earth elements (e.g. Bau, 1996; Irber, 1999) and low K/Rb ratios (Shaw, 1968; Clarke, 1992), are all absent in the rhyolitic rocks (Fig. 4c; Appendix B Fig. S3), also precluding significant fluid-melt/rock interaction for the studied samples. Therefore, we argue that the rhyolitic rocks did not experience extensive fluid-melt/rock interaction and therefore fluid exsolution is unlikely to be the main cause for heavy Fe isotope compositions of the eruptive rocks.

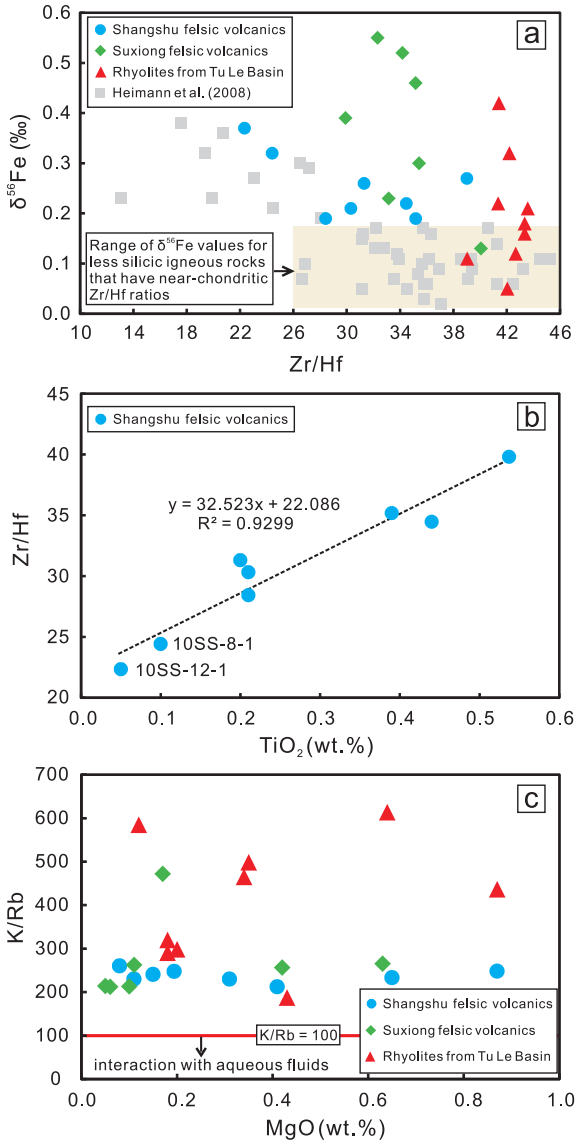

Fig. 4. (a) Plot of whole-rock Zr/Hf ratios versus δ^{56}Fe values for the studied samples. The shaded area represents the range of δ^{56}Fe values for less silicic igneous rocks ($\delta^{56}Fe = 0.09 \pm 0.08‰$; Heimann et al., 2008) that have near-chondritic Zr/Hf ratios (26–46; Bau, 1996). (b) Plot of whole-rock TiO_2 versus Zr/Hf for the studied samples. (c) Plot of MgO versus K/Rb for the rhyolitic rocks. K/Rb ratios <100 are indicative of interaction with aqueous fluids (Clarke, 1992).

Although geochemical indicators rule out extensive fluid-melt/rock interaction, volcanic degassing did occur to the rhyolites upon eruption, and its influence on Fe isotope budget of the rhyolite needs to be quantified. Fe isotope exchange between melt and exsolved vapor during volcanic degassing can be modeled using a Rayleigh fractionation equation:

$$\delta^{56}Fe_{melt} = (\delta^{56}Fe_{initial\ melt} + 1000) \times f^{(\alpha-1)} - 1000 \quad (1)$$

where α is the Fe isotope fractionation factor between melt and vapor ($\alpha = (^{56}Fe/^{54}Fe)_{vapor}/(^{56}Fe/^{54}Fe)_{melt}$) and f is the mass fraction of iron in the residual melt ($f = F_{melt} \times C_{melt}/C_0$, where F_{melt} is the mass fraction of residual melt, C_{melt} is the iron abundance in melt and C_0 is the initial Fe abundance in magma). We assume that the initial melt has a $\delta^{56}Fe$ value of 0.1‰ that is identical to undifferentiated silicic igneous rocks (Heimann et al., 2008; Foden et al., 2015; Wu et al., 2017). The Fe isotope fractionation factor between magnetite and iron in fluid ($\Delta^{56}Fe_{Mag-fluid} = 0.28‰ \times 10^6/T^2$) was derived by Heimann et al. (2008) based on theoretically calculated reduced partition function ratios (or β-factors) for magnetite and aqueous Fe^{2+}(Schauble et al., 2001; Polyakov et al., 2007). Sossi et al. (2012) defined a function of Fe isotope fractionation between magnetite and melt ($\Delta^{56}Fe_{Mag-melt} = 0.13‰ \times 10^6/T^2$). Thus, the fluid-melt Fe isotope fractionation factor can be derived as:

$$\begin{aligned} 1000\ln\alpha &\approx \Delta^{56}Fe_{fluid-melt} \\ &= \Delta^{56}Fe_{Mag-melt} - \Delta^{56}Fe_{Mag-fluid} \\ &= -0.15‰ \times 10^6/T^2 \end{aligned} \quad (2)$$

The negative Fe isotope fractionation factor between fluid and melt indicates that magma degassing will produce high $\delta^{56}Fe$ values in residual melt. Iron isotope fractionation factors can be calculated at given magma temperatures following Eq. (2). Iron content in the residual melt during volcanic degassing can be calculated using a Rayleigh fractionation model:

$$C_{melt}/C_0 = (1 - F_{vapor})^{(D_{vapor/melt}-1)} \quad (3)$$

where F_{vapor} is the mass fraction of the released fluids that can be calculated by subtracting the fraction of residual melt from the system ($F_{vapor} + F_{melt} = 1$), and the $D_{vapor/melt}$ refers to partition coefficient of Fe between vapor and melt. $\delta^{56}Fe$ of melt can be calculated as a function of the mass fraction of released vapor, and Eq. (1) can be expressed as:

$$\begin{aligned} \delta^{56}Fe_{melt} = (&\delta^{56}Fe_{initial\ melt} \\ &+ 1000)[(1 - F_{vapor})^{D_{vapor/melt}}]^{(\alpha-1)} - 1000 \end{aligned} \quad (4)$$

$D_{vapor/melt}$ varies from 0.22 to 3.83 as determined from laboratory experiments on rhyolite systems (Simon et al., 2004), which are in good agreement with the direct measurements from co-existing vapor and glass melt inclusions in natural samples (0.42 to 3.5; Zajacz et al., 2008). For a conservative calculation, we use the maximum $D_{vapor/melt}$ of 3.83 for vapor to explore the largest $\delta^{56}Fe$ variation during degassing. Bulk rock zircon saturation geothermometry (T_{Zr}) is used to estimate the magma temperature (Watson and Harrison, 1983). Calculated T_{Zr} for rocks from the Shangshu Formation, Suxiong Formation and the Tu Le Basin are within the ranges of 782–845 °C, 816–890 °C and 931–1059 °C, respectively. T_{Zr} provides a minimum estimate of magma temperature for rocks that lack inherited zircon, while it suggests a maximum magma temperature for inherited zircon-rich rocks (Miller et al., 2003). Because of the lack of inherited zircon grains in all of the three rock suites, the calculated T_{Zr} represents the minimum magma temperature, and because isotope fractionation factor decreases with increasing temperature, the minimum temperatures for each volcanic series were used in Eq. (2) to calculate the fractionation factors between fluid and magma to explore the largest possible Fe isotope variation caused by fluid exsolution.

The results of magma degassing modeling show that $\delta^{56}Fe$ in residual melt increases with increasing degree of

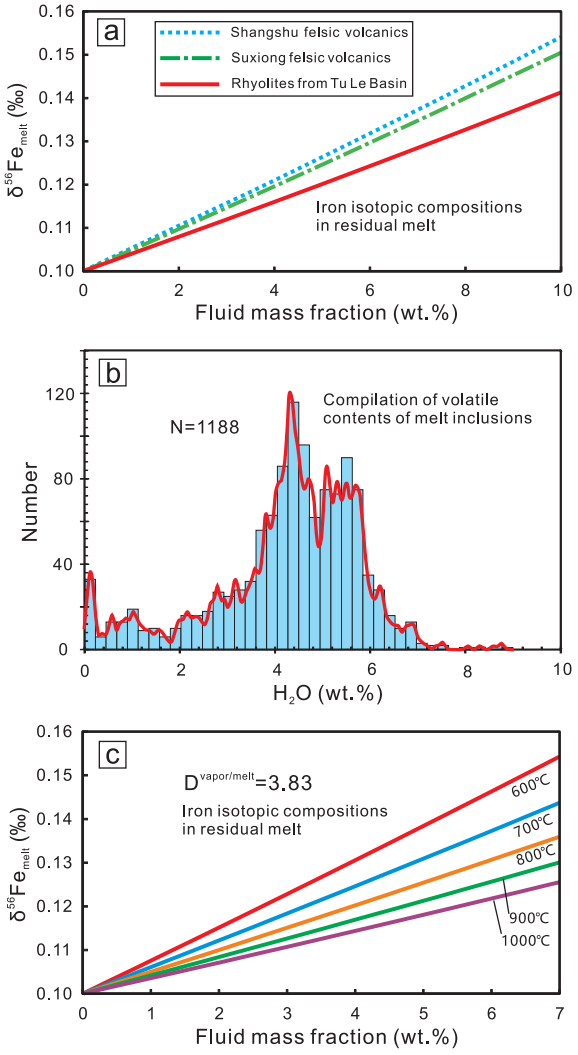

Fig. 5. Rayleigh fractionation model for $\delta^{56}Fe$ of residual melt and fluid mass fraction released from melt during volcanic degassing. (a) The curves for the three studied volcanic suites were calculated combining the Fe isotope fractionation factors between fluid and melt at 782 °C (Shangshu Formation), 816 °C (Suxiong Formation) and 931 °C (Tu Le Basin) of −0.135‰, −0.126‰ and −0.103‰, respectively, with Fe fluid-melt partition coefficient of 3.83. The initial melt is assumed to have $\delta^{56}Fe$ value of 0.1‰. (b) Compilation of volatile contents of melt inclusions in rhyodacite-rhyolites from GEOROC database. (c) The five curves were calculated combining the fluid-melt iron fractionation factors at 600 °C, 700 °C, 800 °C, 900 °C and 1000 °C of −0.197‰, −0.158‰, −0.130‰, −0.109‰ and −0.093‰, with the same partition coefficient between fluid and melt.

degassing (Fig. 5a). The key message from the modeling, however, is that the maximum shift in $\delta^{56}Fe$ of residual melt does not exceed 0.06‰ even if the mass fraction of vapor is up to 10 wt% (Fig. 5a). According to a compilation of volatile contents of melt inclusions in rhyodacite and rhyolites from the GEOROC database (Fig. 5b, http://georoc.mpch-mainz.gwdg.de/georoc/), the majority of melt inclusions have volatile contents of 3–6 wt%, and volatile contents of very few melt inclusions exceed 7 wt%. On the other hand, the magnitude of Fe isotope fractionation increases with decreasing temperature, but even if degassing temperature decreases to 600 °C (Fig. 5c), the modeled Fe isotope variation is still too small to explain the observed $\delta^{56}Fe$ values of up to 0.5‰. Therefore, based on our current understanding of Fe isotope partitioning between volatiles and magmas, contributions of volatile degassing to Fe isotope variation in high-silica volcanic rocks is very limited, and processes other than fluid exsolution are necessary to explain the observed Fe isotopic variation in the rhyolitic rocks.

5.3. Fractional crystallization versus partial melting: the key for iron isotope fractionation in high SiO_2 rocks

Because Soret effect, thermal diffusion and volcanic degassing are all unlikely to be responsible for the large Fe isotope variations observed in the rhyolitic rocks as discussed above, magmatic differentiation and partial melting are left as the two remaining possible mechanisms. Heimann et al. (2008) and Foden et al. (2015) argued that partial melting does not generate significant iron isotope fractionation for low SiO_2 (<70 wt%) felsic magmas and one cannot clearly distinguish I-type from S-type granitoids in terms of Fe isotopes (Telus et al., 2012). In migmatites, the higher $\delta^{56}Fe$ values of leucosomes relative to melanosomes indicate that partial melting of the crust can fractionate Fe isotopes (Telus et al., 2012) but the heavy Fe isotope compositions of leucosomes can also be the product of local accumulation of feldspar that is high in $\delta^{56}Fe$ values but low in Fe contents (Wu et al., 2017). Xu et al. (2017) proposed that crustal anatexis without feldspar accumulation could cause detectable Fe isotope fractionation of ~ 0.09‰ ($\Delta^{56}Fe_{leucosome\text{-}melanosome}$), Fe isotope variation caused by partial melting alone, therefore, is too small to explain the observed $\delta^{56}Fe$ variations for high-silica granitic rocks and the investigated rocks of this study. Crustal assimilation/contamination can also be regarded as a specific form of partial melting that happens at shallower crustal levels, but in this study, the $\delta^{56}Fe$ values of the three volcanic suites show clear correlations with $Fe_2O_3^t$, MgO, Eu/Eu^*, and Sr (Fig. 3, Fig. 7), indicating limited effects of source heterogeneity on Fe isotope variations.

Fractional crystallization of minerals plays a key role in magma evolution towards high-SiO_2 compositions, and may be the dominant factor responsible for Fe isotope fractionation in silicic magmatic systems. Iron possesses two oxidation states (as $Fe^{2+}$and Fe^{3+}) in melts and igneous rocks, in which Fe^{3+}sites tend to enrich heavy Fe isotopes over Fe^{2+}sites (Schauble, 2004; Dauphas et al., 2014; Wu et al., 2017). Calculations based on Mössbauer and NRIXS spectroscopic data suggest that $\delta^{56}Fe$ of minerals under isotope equilibrium increases with Fe^{3+}/Fe^{tot} following the order of hematite > magnetite > pyroxene > ilmenite (Polyakov and Mineev, 2000; Polyakov et al., 2007; Dauphas et al., 2012). In addition, as compiled in Fig. 6, the average $\delta^{56}Fe$ values of mineral separates from igneous rocks distribute in a sequence of plagioclase (0.91 ± 0.33‰; 1SD, $n = 4$) > K-feldspar (0.88 ± 0.16‰; 1SD, $n = 4$) > magnetite (0.29 ± 0.17‰; 1SD, $n = 80$) > biotite (0.07 ± 0.07‰; 1SD, $n = 23$) > amphibole (0.05 ± 0.04‰; 1SD, $n = 8$) > orthopyroxene (-0.03 ± 0.07‰; 1SD, $n = 12$) > clinopyroxene (-0.06 ± 0.07‰; 1SD, $n = 22$) > olivine (-0.15 ± 0.23‰; 1SD, $n = 65$) > ilmenite (-0.23 ± 0.13‰; 1SD, $n = 20$) (Heimann et al., 2008; Sossi et al., 2012; Telus et al., 2012; Chen et al., 2014; Wu et al., 2017; Bilenker et al., 2017). Significant inter-mineral Fe isotope fractionation occurs in magmatic systems, and when this process is combined with a Rayleigh process of fractional crystallization, remarkable modifications of Fe isotope composition of the residual melt could occur.

It is crucial to know which mineral is dominant in controlling Fe isotope fractionation for a certain melt. Whole-rock $\delta^{56}Fe$ values of rhyolites investigated in this study are negatively correlated with $Fe_2O_3^t$ (Fig. 3b), suggesting loss of minerals with isotopically light Fe by fractional crystallization or accumulation of heavy Fe isotopes in residual melts. Olivine and pyroxene cannot be the dominant minerals controlling Fe isotope fractionation in rhyolites because they generally do not crystallize from felsic magmas and they do not drive evident Fe isotopes fractionation in mafic-intermediate igneous rocks, as shown in the $\delta^{56}Fe$-SiO_2 plot (Fig. 10). It is necessary to examine whether feldspar accumulation can produce high $\delta^{56}Fe$ values of high-silica igneous rocks because of its high abundance in felsic rocks and its affinity to heavy Fe isotopes (Wu et al., 2017). However, feldspar has very low $Fe_2O_3^t$ contents (i.e., 0.07–0.17 wt% for plagioclase, and 0.03–0.11 wt% for alkaline-feldspar; Wu et al., 2017), and the amount of iron trans-

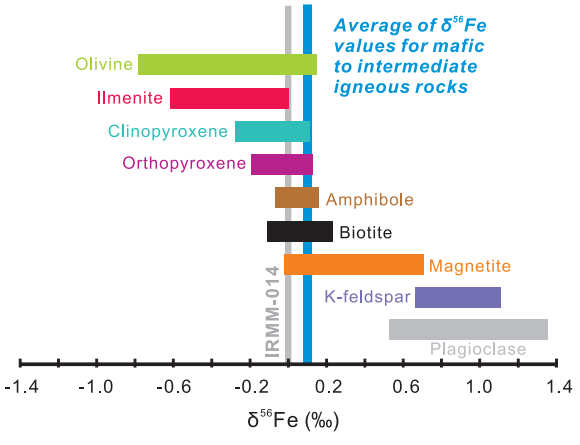

Fig. 6. Compilation of Fe isotope compositions of mineral separates for plagioclase, K-feldspar, magnetite, amphibole, clinopyroxene, orthopyroxene, olivine and ilmenite in literature (data after Heimann et al., 2008; Telus et al., 2012; Sossi et al., 2012; Chen et al., 2014; Bilenker et al., 2017; Wu et al., 2017).

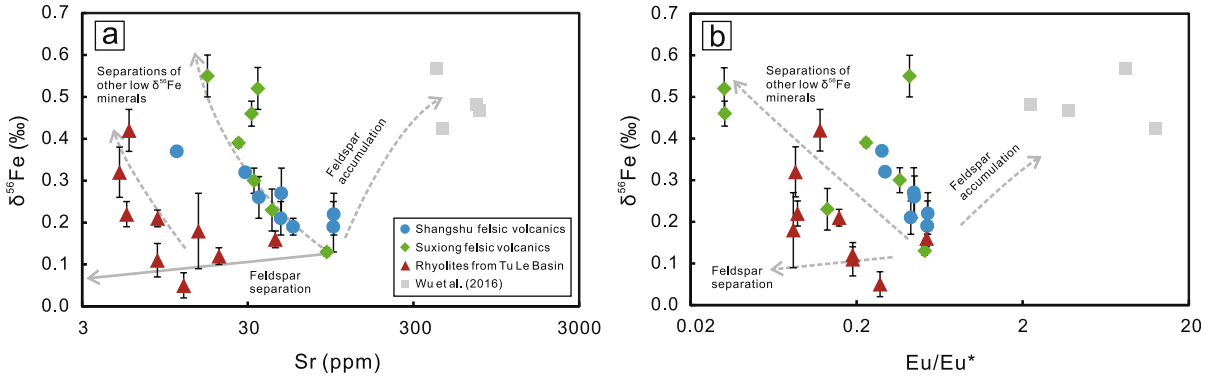

Fig. 7. Sr–δ^{56}Fe (a) and Eu/Eu*–δ^{56}Fe (b) diagrams showing the role of feldspar in controlling iron isotopic fractionations. The grey solid line shows the predicted Rayleigh path of the melt expected from feldspar crystallization and removal by assuming a feldspar-melt fractionation factor of 0.8‰ based on the data of Wu et al. (2017). The dacitic sample from Suxiong Formation (15SX-12-1) was adopted as initial component (Sr = 89.9 ppm, $Fe_2O_3^t$ = 4.07 wt%, δ^{56}Fe = 0.13‰). The partition coefficients of Sr and Fe between feldspar (including K-feldspar and Plagioclase) and melt were set as 10 and 0.2, respectively (Ewart and Griffin, 1994). The other trends were drawn schematically, and particularly the trend of "Feldspar accumulation" was drawn following the plots in He et al. (2017).

ferred by separation of feldspar is small compared with the high and variable $Fe_2O_3^t$ (0.78–4.31 wt%) in the investigated samples in this study. Moreover, petrographic evidence of feldspar accumulation is lacking in the investigated rhyolite samples (Appendix B Fig. S1), instead the strong depletions of Ba, Sr and Eu suggest the rhyolite magma has experienced crystal fractionation (Fig. 7). Fractional crystallization of feldspars should drive the evolving melt towards lower δ^{56}Fe values (Fig. 7a), but because of the low Fe contents in feldspars, such isotopic effect should be insignificant (Fig. 7a). Only separation of isotopically light Fe-Mg silicates and Fe-Ti oxides can result in significant changes in both Fe contents and Fe isotope compositions of the melts.

Amphibole and titanite are the other possible phases that can separate from silicic magmas by fractional crystallization, and partitioning of light Fe isotopes into these phases in combination of fractional crystallization theoretically could produce enrichment of heavy Fe isotopes in evolved melts. It should be noted that amphibole and titanite have higher distribution coefficients for middle REEs than light REEs and heavy REEs (e.g., Sisson, 1994; Bachmann et al., 2005). Thus separation of amphibole and titanite from melt would induce depletions of middle REEs in the residual melt with a U-shaped REE pattern (Glazner et al., 2008; Streck, 2014). However, Chondrite-normalized REE patterns of our samples show a slightly right-inclining shape with a negative Eu anomaly (Appendix B Fig. S3), ruling out significant fractional crystallizations of amphibole and titanite in these rocks.

Based on the above discussions, the possible minerals for producing high δ^{56}Fe magma narrow down to Fe-Ti oxides and biotite. The three volcanic suites display decreases in $Fe_2O_3^t$ and TiO_2 with increasing SiO_2 and a positive correlation between $Fe_2O_3^t$ and TiO_2 (Fig. 8a), indicating fractional crystallization of Fe-Ti oxides, such as titanomagnetite and ilmenite (Li et al., 2002; Tran et al., 2015). Iron isotope fractionation between titanomagnetite and corresponding melt is dependent on the mag-

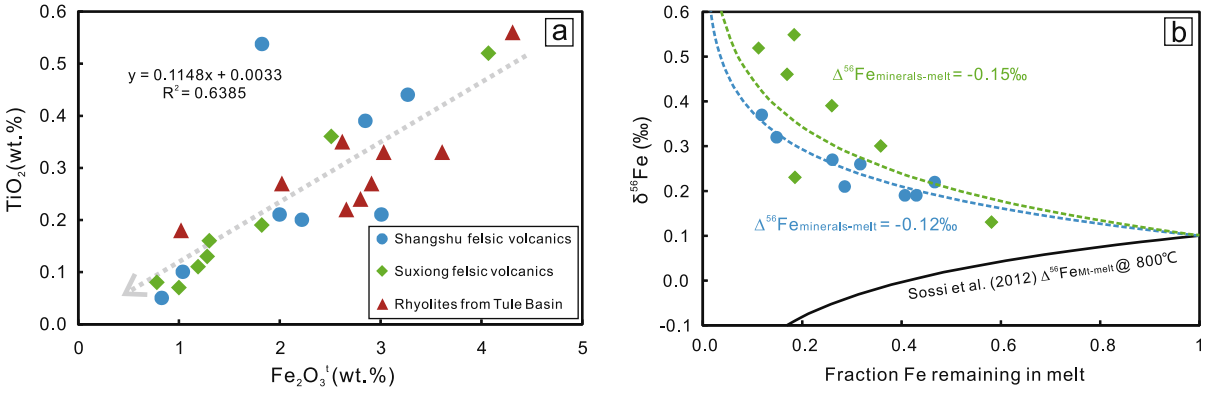

Fig. 8. (a) Plot of whole-rock $Fe_2O_3^t$ versus TiO_2 for the studied samples. (b) Modeling of Fe isotope variations during fractional crystallization in the Shangshu and Suxiong formations. The green curve is the apparent best fit for the Suxiong data with a bulk mineral-melt fractionation factor of −0.15‰. The blue is the best fit for the Shangshu data with a fractionation factor of −0.12‰. The black curve illustrates the effect of magnetite crystallization and separation. (For interpretation of the references to colour in this figure legend, the reader is referred to the web version of this article.)

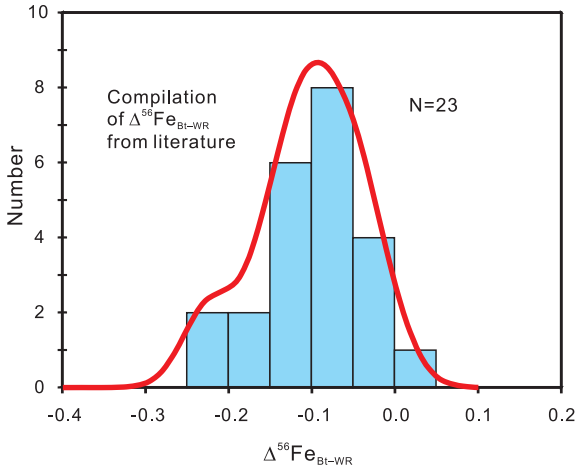

Fig. 9. Compilation of $\Delta^{56}Fe_{Bt-WR}$ from literatures (Heimann et al., 2008; Telus et al., 2012; Wu et al., 2017). Bt = biotite, WR = whole rock, $\Delta^{56}Fe_{Bt\text{-}WR} = \delta^{56}Fe_{Bt} - \delta^{56}Fe_{WR}$.

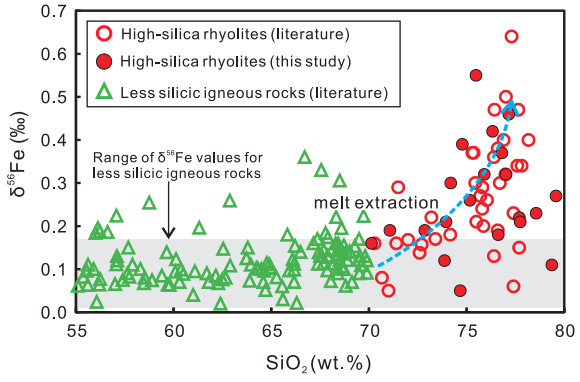

Fig. 10. Plot of SiO_2 versus $\delta^{56}Fe$ of less silicic igneous rocks. Literature data are from Foden et al. (2015), Heimann et al. (2008), Schuessler et al. (2009), Zambardi et al. (2014), Telus et al. (2012), Sossi et al. (2012), Gajos et al. (2016), He et al. (2017) and Xia et al. (2017). The shaded area represents the range of $\delta^{56}Fe$ values for less silicic igneous rocks (0.09 ± 0.08‰; Heimann et al., 2008).

netite/ulvöspinel ratio (Sossi et al., 2012). The fractionation factor between nearly pure magnetite (~Mag_{95}) and melt based on a case study from Red Hill is positive ($\Delta^{56}Fe_{Mag-melt} = 0.13‰ \times 10^6/T^2$; Sossi et al., 2012). Furthermore, it was also reported that magnetite-rich titanomagnetite (~Mag_{67}) is enriched in heavy Fe isotopes ($\delta^{56}Fe = 0.20$ to 0.31‰; Liu et al., 2014) relative to mafic-intermediate igneous rocks ($\delta^{56}Fe = 0.09 \pm 0.08$‰; Heimann et al., 2008). These observations suggest that significant fractional crystallization of magnetite-rich titanomagnetite would lead to depletion of heavy Fe isotopes in residual magma, which is opposite to our observation (Fig. 8b). Although no experimental data of Fe isotope fractionation is available for pure ulvöspinel, Schuessler et al. (2009) proposed that the high-$\delta^{56}Fe$ rhyolites from Hekla volcano were produced by removal of ulvöspinel-rich titanomagnetite (~Mag_{35}, Baldridge et al., 1973) with a mineral-melt fractionation factor of around –0.1‰. Besides, both theoretical calculations and observations of natural samples indicate that ilmenite is enriched in light iron isotopes (Fig. 6, Polyakov and Mineev, 2000; Chen et al., 2014). The negative fractionation factor between Fe-Ti oxides (ulvöspinel-rich titanomagnetite and/or ilmenite) and melt in combination with positive correlation between $Fe_2O_3^t$ and TiO_2 (Fig. 8a) suggests a possible role of fractional crystallization of these minerals in producing high $\delta^{56}Fe$ magma. In addition, mineral separates of biotite from granites show $\delta^{56}Fe$ ranging from –0.05‰ to 0.18‰ (Fig. 6, Heimann et al., 2008; Telus et al., 2012; Wu et al., 2017), slightly below or comparable to their whole rocks ($\Delta^{56}Fe_{Bt-Whole\ rock} = 0.001‰$ to $-0.23‰$; Fig. 9). Gajos et al. (2016) suggested a $\Delta^{56}Fe_{Bt-melt}$ of $-0.02‰$ assuming all biotites crystallized from a melt of mean mafic composition ($\delta^{56}Fe = +0.09‰$; Beard and Johnson, 2004). But we argue that such fractionation factor may be underestimated because most of biotite-bearing felsic rocks show heavier bulk rock Fe isotope compositions (0.067–0.36‰, $\delta^{56}Fe_{average} = 0.17‰$; Heimann et al., 2008; Telus et al., 2012; Wu et al., 2017) than mean mafic rock compositions ($\delta^{56}Fe = +0.09‰$; Beard and Johnson, 2004). The fractionation factor between biotite and melt was re-estimated as $-0.1‰$ based on average $\Delta^{56}Fe_{Bt-Whole\ rock}$ from two volcanic rocks and twenty-one plutonic rocks (Fig. 9; Heimann et al., 2008; Telus et al., 2012; Wu et al., 2017), suggesting that fractional crystallization of biotite could also play a role in producing high $\delta^{56}Fe$ values of high-silica rhyolites.

The integrated Fe isotope fractionation effects of these minerals can be estimated using a Rayleigh fractionation model based on Eq. (1). The initial Fe content of the melt was set at 5 wt% based on measured Fe contents in the investigated rhyolitic rocks. Calculations show that the Fe isotope signatures of volcanic rocks from the Shangshu and Suxiong formations can be produced by fractional crystallization with a mineral-melt fractionation factor $\Delta^{56}Fe_{mineral-melt}$ of $-0.12‰$ and $-0.15‰$, respectively (Fig. 8b). However, the correlation between $\delta^{56}Fe$ and $Fe_2O_3^t$ for the rhyolitic rocks from the Tu Le Basin is poor and cannot be reconciled with a simple Reyleigh model, which implies that the crystallization/eruptive history of the Tu Le rhyolitic rocks may be more complicated than fractional crystallization of ulvöspinel-rich titanomagnetite, ilmenite and biotite.

The variation in modeled fractionation factors in Fig. 8b may reflect differences in magma compositions and mineral assemblages during magma differentiation. On the one hand, the Suxiong rhyolites have higher molar (K + Na)/(Ca + Mg) ratios (4–41) relative to the Shangshu rhyolites (3–18, excluding an anomalous sample of 10SS-12-1), and a larger fractionation factor between melt and minerals ($\Delta^{56}Fe_{melt-mineral}$) may be associated with higher (K + Na)/(Ca + Mg) ratio because alkaline cations in magma tend to stabilize Fe cations with low coordination numbers (He et al., 2017). On the other hand, Fe isotope fractionation factors may also be affected by mineral assemblages of fractional crystallization as a function of magma composition and the crystallization condition, and the Suxiong rhyolites may have experienced more significant fractional

crystallization of Fe-Ti oxides (especially ilmenite) than the Shangshu rhyolites. Fractional crystallization of the Fe^{2+}-enriched minerals may reflect that the three volcanic suites crystallized under relatively reduced conditions regardless of whether the system was closed or opened to oxygen exchange (Sossi et al., 2012; Foden et al., 2015). It should be noted that Foden et al. (2015) argued that late Fe-Mg silicate fractionation in an oxidized system that is closed to oxygen exchange can also drive the residual melt to a late heavy Fe isotope enrichment.

Consequently, we conclude that partitioning of light Fe isotopes into Fe-Ti oxides (ulvöspinel-rich titanomagnetite, ilmenite) and biotite in combination with the subsequent separation of these minerals by fractional crystallization from magma best explains the observed heavy Fe isotope compositions in high-silica rhyolites.

5.4. Implications for magmatic evolution and iron isotope fractionation in high-SiO_2 rhyolite

Based on the discussions above, crystal-liquid separation (fractional crystallization) is the most likely mechanism for explaining the high $\delta^{56}Fe$ values in high-silica rhyolites. However, the physical processes associated with crystal-liquid separation (fractional crystallization) remain controversial, because felsic magmas have high viscosity and the crystallizing minerals (e.g., quartz, feldspar, mica) have densities similar to co-existing melts (Wickham, 1987; Clemens and Petford, 1999; Zhang, 2012). Thus, generation of the high-silica rhyolites magma by crystal settling as in mafic magma chambers seems to be insufficient. Different from crystal settling by density contrast in mafic magma, high-silica rhyolites are thought to be generated by melt extraction from a crystal mush of intermediate-silicic compositions in upper crust at crystallinities of ~50–60 vol.% (e.g. Bachmann and Bergantz, 2004, 2008; Bachmann et al., 2005; Glazner et al., 2008; Deering et al., 2011; Lee and Morton, 2015). When the crystal fraction approaches ~50–60 vol.%, the remaining interstitial melt has high-silica, and the crystal-liquid system locks up and begins to exhibit solid behavior rheologically, preventing turnover or convection (Bachmann and Bergantz, 2004, 2008) but allowing melt extraction to begin. Consequently, the escaping high-silica rhyolitic melt accumulates in the upper part of the magma chamber and produces a crystal-poor melt cap that ultimately leads to eruption (Bachmann and Bergantz, 2004). It is important to note that Rayleigh process still applies to the system during melt extraction because chemical equilibrium is difficult to attain between crystals and melt, particularly in cold magmas and for slow diffusing species, such as REE, Sr, Ba and Zr (Bachmann and Bergantz, 2004; Deering and Bachmann, 2010; Bachmann et al., 2014; Lee and Morton, 2015).

Generation of crystal-poor high-SiO_2 rhyolites always leaves a complementary reservoir of accumulates (Deering and Bachmann, 2010) that are most likely preserved as granodioritic batholiths and sometimes crystal-rich ignimbrites (Bachmann and Bergantz, 2004). However, it is difficult to identify the reservoir of accumulates because they actually are mixtures of crystals and interstitial high-Si silicic melt, resulting them geochemically similar to high-Si rhyolites (Deering and Bachmann, 2010; Gelman et al., 2014; Lee and Morton, 2015). Interestingly, most of high-silica rhyolites have $\delta^{56}Fe$ values that are significantly higher than those of less silicic igneous rocks. Furthermore, the aforementioned discussions suggest that degassing has a limited contribution to iron isotopic variation in high-silica volcanic rocks but the removal of some specific mineral phases do. Thus, iron isotopes may be a powerful tool in tracking magmatic processes for high-silica rhyolites. As shown in Fig. 10, less silicic (55–70 wt% SiO_2) rocks have $\delta^{56}Fe$ values that mostly vary within the range of mafic-intermediate igneous rocks ($0.09 \pm 0.08‰$; Beard et al., 2003; Poitrasson and Freydier, 2005; Heimann et al., 2008), but most of high-silica rhyolites have higher $\delta^{56}Fe$ values (Heimann et al., 2008; Schuessler et al., 2009; Zambardi et al., 2014; this study). This trend can be explained by crystal mush extraction model, in which less silicic rocks may stand for the primary melt of high-silica rhyolite or accumulates with high-silica interstitial melt, while high-silica rhyolites may represent the interstitial liquid extracted from crystal mush (Fig. 10). This hypothesis can be tested using mass-balance equations:

$$\delta^{56}Fe_{initial} = \delta^{56}Fe_{cum} \cdot X_{cum} + \delta^{56}Fe_{int} \cdot X_{int} + \delta^{56}Fe_{ext} \cdot X_{ext} \quad (6)$$

where X_{cum}, X_{int} and X_{ext} are the mass fraction of iron in cumulates, trapped interstitial melt and extracted melt, respectively. Thus $\delta^{56}Fe$ values of accumulates with high-silica interstitial melt can be calculated by:

$$\delta^{56}Fe_{cum} \cdot X_{cum} + \delta^{56}Fe_{int} \cdot X_{int} = \delta^{56}Fe_{initial} - \delta^{56}Fe_{ext} \cdot X_{extra} \quad (7)$$

At 50–60% crystallization, the interstitial melt is rhyolitic and no more than 70–80% of the interstitial melt can be extracted (Lee and Morton, 2015). Assuming iron contents of initial and extracted melt are 5 wt% and 2 wt%, respectively, and $\delta^{56}Fe$ value of extracted melt is 0.4‰ as most published rhyolite $\delta^{56}Fe$ values do not exceed this value (Fig. 10), mass balance indicates that the shift in the Fe isotopic composition of the residue (cumulates + trapped melt) caused by extraction of high-silica rhyolite will not exceed 0.06‰. This could explain why less silicic rocks have relatively homogeneous iron isotopic compositions while the high-silica rhyolites can have high $\delta^{56}Fe$ values.

6. CONCLUSIONS

Mechanisms of Fe isotope fractionation in high-SiO_2 volcanic rocks were investigated based on rhyolitic rocks from the Neoproterozoic volcanic-sedimentary sequences in southern China and the Triassic Tu Le Basin in northern Vietnam. These rocks show very large variation in $\delta^{56}Fe$ values in igneous rocks (from $0.05 \pm 0.05‰$ to $0.55 \pm 0.05‰$). Modeling results suggest that fluid exsolution during magma degassing contributes little to Fe isotope fractionation in bulk rocks, and the Fe isotope variations in the investigated samples cannot be caused by Soret effect and thermal diffusion. Partial melting or source heterogene-

ity are also ruled out as the cause of high δ^{56}Fe signatures in the rocks. Fractional crystallization of Fe-Ti oxides (e.g. ulvöspinel-rich titanomagnetite and ilmenite) and biotite is proposed as the dominant driving mechanism for the remarkable enrichment of heavy iron isotopes in the studied rocks. This study provides solid evidence for fractional crystallization as the dominant factor that controls iron isotope fractionation of high-silica rhyolitic magmas. The mechanism may also play an important role in causing the large Fe isotope variation in other high-silica intrusive rocks and it can potentially serve as a useful tool in tracking magmatic differentiation for high-silica melts.

ACKNOWLEDGMENTS

This manuscript benefits from constructive reviews from Adriana Heimann, John Foden, and an anonymous reviewer. We also thank Dr. Fangzhen Teng for his editorial handling and constructive comments. This work was financially supported by the State Key R&D Project of China (2016YFC0600203) and National Natural Science Foundation of China (41472049) to XLW, and "1000-talents program" of China to WL.

APPENDIX A. SUPPLEMENTARY DATA

Supplementary data associated with this article can be found, in the online version, at http://dx.doi.org/10.1016/j.gca.2017.09.014.

REFERENCES

Bachmann O. and Bergantz G. W. (2004) On the origin of crystal-poor rhyolites: extracted from batholithic crystal mushes. *J. Petrol.* **45**, 1565–1582.

Bachmann O. and Bergantz G. W. (2008) Rhyolites and their source mushes across tectonic settings. *J. Petrol.* **49**, 2277–2285.

Bachmann O., Deering C. D., Lipman P. W. and Plummer C. (2014) Building zoned ignimbrites by recycling silicic cumulates: insight from the 1000 km^3 Carpenter Ridge Tuff, CO. *Contrib. Mineral. Petrol.* **167**, 1025.

Bachmann O., Dungan M. A. and Bussy F. (2005) Insights into shallow magmatic processes in large silicic magma bodies: the trace element record in the Fish Canyon magma body, Colorado. *Contrib. Mineral. Petrol.* **149**, 338–349.

Baker D. R. and Alletti M. (2012) Fluid saturation and volatile partitioning between melts and hydrous fluids in crustal magmatic systems: the contribution of experimental measurements and solubility models. *Earth-Sci. Rev.* **114**, 298–324.

Baldridge W. S., McGetchin T. R., Frey F. A. and Jarosewich E. (1973) Magmatic evolution of Hekla, Iceland. *Contrib. Mineral. Petrol.* **42**, 245–258.

Bau M. (1996) Controls on the fractionation of isovalent trace elements in magmatic and aqueous systems: evidence from Y/Ho, Zr/Hf, and lanthanide tetrad effect. *Contrib. Mineral. Petrol.* **123**, 323–333.

Bea F., Montero P. and Ortega M. (2006) A LA–ICP–MS evaluation of Zr reservoirs in common crustal rocks: Implications for Zr and Hf geochemistry, and zircon-forming processes. *Can. Mineral.* **44**, 693–714.

Beard B. L. and Johnson C. M. (2004) Inter-mineral Fe isotope variations in mantle-derived rocks and implications for the Fe geochemical cycle. *Geochim. Cosmochim. Acta* **68**, 4727–4743.

Beard B. L., Johnson C. M., Skulan J. L., Nealson K. H., Cox L. and Sun H. (2003) Application of Fe isotopes to tracing the geochemical and biological cycling of Fe. *Chem. Geol.* **195**, 87–117.

Bilenker L. D., Vantongeren J. A., Lundstrom C. C. and Simon A. C. (2017) Iron isotopic evolution during fractional crystallization of the uppermost Bushveld complex layered mafic intrusion. *Geochem. Geophys. Geosyst.*. http://dx.doi.org/10.1002/2016GC006660.

Chen L. M., Song X. Y., Zhu X. K., Zhang X. Q., Yu S. Y. and Yi J. N. (2014) Iron isotope fractionation during crystallization and sub-solidus re-equilibration: Constraints from the Baima mafic layered intrusion, SW China. *Chem. Geol.* **380**, 97–109.

Chung S. L., Lee T. Y., Lo C. H., Wang P. L., Chen C. Y., Yem N. T., Hoa T. T. and Genyao W. (1997) Intraplate extension prior to continental extrusion along the Ailao Shan-Red River shear zone. *Geology* **25**, 311–314.

Clarke D. B. (1992) The mineralogy of peraluminous granites: A review. *Can. Mineral.* **19**, 3–17.

Clemens J. D. and Petford N. (1999) Granitic melt viscosity and silicic magma dynamics in contrasting tectonic settings. *J. Geol. Soc.* **156**, 1057–1060.

Craddock P. R. and Dauphas N. (2011) Iron isotopic compositions of geological reference materials and chondrites. *Geostand. Geoanal. Res.* **35**, 101–123.

Dauphas N., Roskosz M., Alp E. E., Golden D. C., Sio C. K., Tissot F. L. H., Hu M. Y., Zhao J., Gao L. and Morris R. V. (2012) A general moment NRIXS approach to the determination of equilibrium Fe isotopic fractionation factors: application to goethite and jarosite. *Geochim. Cosmochim. Acta* **94**, 254–275.

Dauphas N., Roskosz M., Alp E. E., Neuville D. R., Hu M. Y., Sio C. K., Tissot F. L. H., Zhao J., Tissandier L., Médard E. and Cordier C. (2014) Magma redox and structural controls on iron isotope variations in Earth's mantle and crust. *Earth Planet. Sci. Lett.* **398**, 127–140.

Deering C. D. and Bachmann O. (2010) Trace element indicators of crystal accumulation in silicic igneous rocks. *Earth Planet. Sci. Lett.* **297**, 324–331.

Deering C. D., Cole J. W. and Vogel T. A. (2011) Extraction of crystal-poor rhyolite from a hornblende-bearing intermediate mush: a case study of the caldera-forming Matahina eruption, Okataina volcanic complex. *Contrib. Mineral. Petrol.* **161**, 129–151.

Driesner T. and Heinrich C. A. (2007) The system H_2O–NaCl. Part I: Correlation formulae for phase relations in temperature–pressure–composition space from 0 to 1000° C, 0 to 5000bar, and 0 to 1 X NaCl. *Geochim. Cosmochim. Acta* **71**, 4880–4901.

Ewart A. and Griffin W. L. (1994) Application of proton-microprobe data to trace-element partitioning in volcanic rocks. *Chem. Geol.* **117**, 251–284.

Foden J., Sossi P. A. and Wawryk C. M. (2015) Fe isotopes and the contrasting petro-genesis of A-, I-and S-type granite. *Lithos* **212–215**, 32–44.

Gajos N. A., Lundstrom C. C. and Taylor A. H. (2016) Spatially controlled Fe and Si isotope variations: an alternative view on the formation of the Torres del Paine pluton. *Contrib. Mineral. Petrol.* **11**(171), 1–20.

Gelman S. E., Deering C. D., Bachmann O., Huber C. and Gutiérrez F. J. (2014) Identifying the crystal graveyards remaining after large silicic eruptions. *Earth Planet. Sci. Lett.* **403**, 299–306.

Glazner A. F., Coleman D. S. and Bartley J. M. (2008) The tenuous connection between high-silica rhyolites and granodiorite plutons. *Geology* **36**, 183–186.

He Y., Ke S., Teng F. Z., Wang T., Wu H., Lu Y. and Li S. (2015) High-precision iron isotope analysis of geological reference materials by high-resolution MC-ICP-MS. *Geostand. Geoanal. Res.* **39**, 341–356.

He Y., Wu H., Ke S., Liu S. A. and Wang Q. (2017) Iron isotopic compositions of adakitic and non-adakitic granitic magmas: magma compositional control and subtle residual garnet effect. *Geochim. Cosmochim. Acta* **203**, 89–102.

Heimann A., Beard B. L. and Johnson C. M. (2008) The role of volatile exsolutions and sub-solidus fluid/rock interactions in producing high $^{56}Fe/^{54}Fe$ ratios in siliceous igneous rocks. *Geochim. Cosmochim. Acta* **72**, 4379–4396.

Hill P. S., Schauble E. A. and Young E. D. (2010) Effects of changing solution chemistry on Fe^{3+}/Fe^{2+} isotope fractionation in aqueous Fe–Cl solutions. *Geochim. Cosmochim. Acta* **74**, 6669–6689.

Huang F., Lundstrom C. C., Glessner J., Ianno A., Boudreau A., Li J., Ferré E. C., Mar-shak S. and DeFrates J. (2009) Chemical and isotopic fractionation of wet andesite in a temperature gradient: experiments and models suggesting a new mechanism of magma differentiation. *Geochim. Cosmochim. Acta* **73**, 729–749.

Irber W. (1999) The lanthanide tetrad effect and its correlation with K/Rb, Eu/Eu*, Sr/Eu, Y/Ho, and Zr/Hf of evolving peraluminous granite suites. *Geochim. Cosmochim. Acta* **63**, 489–508.

Lan C. Y., Chung S. L., Jiun-San Shen J., Lo C. H., Wang P. L., Hoa T. T., Thanh H. H. and Mertzman S. A. (2000) Geochemical and Sr–Nd isotopic characteristics of granitic rocks from northern Vietnam. *J. Asian Earth Sci.* **18**, 267–280.

Lee C. T. A. and Morton D. M. (2015) High silica granites: Terminal porosity and crystal settling in shallow magma chambers. *Earth Planet. Sci. Lett.* **409**, 23–31.

Leloup P. H., Lacassin R., Tapponnier P., Schärer U., Zhong D., Liu X., Zhang L., Ji S. and Trinh P. T. (1995) The Ailao Shan-Red River shear zone (Yunnan, China), Tertiary transform boundary of Indochina. *Tectonophysics* **251**, 3–84.

Li X. H., Li W. X., Li Z. X. and Liu Y. (2008) 850–790 Ma bimodal volcanic and intrusive rocks in northern Zhejiang, South China: a major episode of continental rift magmatism during the breakup of Rodinia. *Lithos* **102**, 341–357.

Li X. H., Li Z. X., Zhou H., Liu Y. and Kinny P. D. (2002) U-Pb zircon geochronology, geochemistry and Nd isotopic study of Neoproterozoic bimodal volcanic rocks in the Kangdian Rift of South China: implications for the initial rifting of Rodinia. *Precambrian Res.* **113**, 135–154.

Li X. H., Qi C. S., Liu Y., Liang X. R., Tu X. L., Xie L. W. and Yang Y. H. (2005) Petrogenesis of the Neoproterozoic bimodal volcanic rocks along the western margin of the Yangtze block: new constraints from Hf isotopes and Fe/Mn ratios (in Chinese). *Chinese Sci. Bull.* **50**, 2481–2486.

Linnen R. L. and Keppler H. (2002) Melt composition control of Zr/Hf fractionation in magmatic processes. *Geochim. Cosmochim. Acta* **66**, 3293–3301.

Liu P. P., Zhou M. F., Luais B., Cividini D. and Rollion-Bard C. (2014) Disequilibrium iron isotopic fractionation during the high-temperature magmatic differentiation of the Baima Fe-Ti oxide-bearing mafic intrusion. *SW China. Earth Planet. Sci. Lett.* **399**, 21–29.

Louvel M., Sanchez-Valle C., Malfait W. J., Cardon H., Testemale D. and Hazemann J. L. (2014) Fluids in the crust. Constraints on the mobilization of Zr in magmatic-hydrothermal processes in subduction zones from in situ fluid-melt partitioning experiments. *Am. Mineral.* **99**, 1616–1625.

Lundstrom C. (2009) Hypothesis for the origin of convergent margin granitoids and Earth's continental crust by thermal migration zone refining. *Geochim. Cosmochim. Acta* **73**, 5709–5729.

Miller C. F., McDowell S. M. and Mapes R. W. (2003) Hot and cold granites? Implications of zircon saturation temperatures and preservation of inheritance. *Geology* **31**, 529–532.

Poitrasson F. and Freydier R. (2005) Heavy iron isotope composition of granites deter-mined by high resolution MC-ICP-MS. *Chem. Geol.* **222**, 123–147.

Polyakov V. B. and Mineev S. D. (2000) The use of Mössbauer spectroscopy in stable isotope geochemistry. *Geochim. Cosmochim. Acta* **64**, 849–865.

Polyakov V. B., Clayton R. N., Horita J. and Mineev S. D. (2007) Equilibrium iron isotope fractionation factors of minerals: reevaluation from the data of nuclear inelastic resonant X-ray scattering and Mössbauer spectroscopy. *Geochim. Cosmochim. Acta* **71**, 3833–3846.

Richter F. M., Watson E. B., Mendybaev R., Dauphas N., Georg B., Watkins J. and Valley J. (2009) Isotopic fractionation of the major elements of molten basalt by chemical and thermal diffusion. *Geochim. Cosmochim. Acta* **73**, 4250–4263.

Schauble E. A. (2004) Applying stable isotope fractionation theory to new systems. *Rev. Mineral. Geochem.* **55**, 65–111.

Schauble E. A., Rossman G. R. and Taylor, Jr., H. P. (2001) Theoretical estimates of equilibrium Fe-isotope fractionations from vibrational spectroscopy. *Geochim. Cosmochim. Acta* **65** (15), 2487–2497.

Schuessler J. A., Schoenberg R. and Sigmarsson O. (2009) Iron and lithium isotope systematics of the Hekla volcano, Iceland – evidence for Fe isotope fractionation during magma differentiation. *Chem. Geol.* **258**, 78–91.

Shaw D. M. (1968) A review of K-Rb fractionation trends by covariance analysis. *Geochim. Cosmochim. Acta* **32**, 573–601.

Sigurdsson, H., Houghton, B., McNutt, S., Rymer, H. and Stix, J. (eds.) (2015) *The encyclopedia of volcanoes*. Elsevier.

Simon A. C., Pettke T., Candela P. A., Piccoli P. M. and Heinrich C. A. (2004) Magnetite solubility and iron transport in magmatic-hydrothermal environments. *Geochim. Cosmochim. Acta* **68**, 4905–4914.

Sisson T. W. (1994) Hornblende-melt trace-element partitioning measured by ion microprobe. *Chem. Geol.* **117**, 331–344.

Sossi P. A., Foden J. D. and Halverson G. P. (2012) Redox-controlled iron isotope fractionation during magmatic differentiation: an example from the Red Hill intrusion. *S. Tasmania. Contrib. Mineral. Petrol.* **164**, 757–772.

Streck M. J. (2014) Evaluation of crystal mush extraction models to explain crystal-poor rhyolites. *J. Volcanol. Geotherm. Res.* **284**, 79–94.

Sun S. S. and McDonough W. S. (1989) Chemical and isotopic systematics of oceanic basalts: implications for mantle composition and processes. *Geol. Soc. Lond. Spec. Publ.* **42**, 313–345.

Tapponnier P., Lacassin R., Leloup P., Scharer U., Zhong D. L., Wu H. W., Liu X. H., Ji S. C., Zhang L. S. and Zhong J. Y. (1990) The Ailaoshan/Red River metamorphic belt: tertiary left lateral shear between Indochina and South China. *Nature* **343**, 431–437.

Telus M., Dauphas N., Moynier F., Tissot F. L. H., Teng F. Z., Nabelek P. I., Craddock P. R. and Groat L. A. (2012) Iron, zinc, magnesium and uranium isotopic fractionation during continental crust differentiation: the tale from migmatites, granitoids, and pegmatites. *Geochim. Cosmochim. Acta* **97**, 247–265.

Teng F. Z., Dauphas N., Huang S. and Marty B. (2013) Iron isotopic systematics of oceanic basalts. *Geochim. Cosmochim. Acta* **107**, 12–26.

Teng F. Z., McDonough W. F., Rudnick R. L., Walker R. J. and Sirbescu M. L. C. (2006) Lithium isotopic systematics of granites and pegmatites from the Black Hills, South Dakota. *Am. Mineral.* **91**, 1488–1498.

Tran T. H., Lan C. Y., Usuki T., Shellnutt J. G., Pham T. D., Tran T. A., Pham N. C., Ngo T. P., Izokh T. P. and Borisenko A. S. (2015) Petrogenesis of Late Permian silicic rocks of Tu Le Basin and Phan Si Pan uplift (NW Vietnam) and their association with the Emeishan large igneous province. *J. Asian Earth Sci.* **109**, 1–19.

Wang J. and Li Z. X. (2003) History of Neoproterozoic rift basins in South China: implications for Rodinia break-up. *Precambrian Res.* **122**, 141–158.

Wang X. L., Shu L. S., Xing G. F., Zhou J. C., Tang M., Shu X. J., Qi L. and Hu Y. H. (2012) Post-orogenic extension in the eastern part of the Jiangnan orogen: evidence from ca 800–760Ma volcanic rocks. *Precambrian Res.* **222**, 404–423.

Wang X. L., Zhou J. C., Griffin W. L., Zhao G. C., Yu J. H., Qiu J. S., Zhang Y. J. and Xing G. F. (2014) Geochemical zonation across a Neoproterozoic orogenic belt: Isotopic evidence from granitoids and metasedimentary rocks of the Jiangnan orogen. *China. Precambrian Res.* **242**, 154–171.

Wang X. L., Zhou J. C., Qiu J. S., Jiang S. Y. and Shi Y. R. (2008) Geochronology and geochemistry of Neoproterozoic mafic rocks from western Hunan, South China: implications for petrogenesis and post-orogenic extension. *Geol. Mag.* **145**, 215–233.

Watson E. B. and Harrison T. M. (1983) Zircon saturation revisited: temperature and composition effects in a variety of crustal magma types. *Earth Planet. Sci. Lett.* **64**, 295–304.

Wawryk C. M. and Foden J. D. (2015) Fe-isotope fractionation in magmatic-hydrothermal mineral deposits: a case study from the Renison Sn–W deposit. *Tasmania. Geochim. Cosmochim. Acta* **150**, 285–298.

Webster J. D. and Holloway J. R. (1990) Partitioning of F and Cl between magmatic hydrothermal fluids and highly evolved granitic magmas. *Geological Society of America Special Papers* **246**, 21–34.

Webster J. D., Holloway J. R. and Hervig R. L. (1989) Partitioning of lithophile trace elements between H_2O and H_2O+CO_2 fluids and topaz rhyolite melt. *Econ. Geol.* **84**, 116–134.

Wickham S. M. (1987) The segregation and emplacement of granitic magmas. *J. Geol. Soc.* **144**, 281–297.

Wilke M., Schmidt C., Dubrail J., Appel K., Borchert M., Kvashnina K. and Manning C. E. (2012) Zircon solubility and zirconium complexation in $H_2O + Na_2O + SiO_2 + Al_2O_3$ fluids at high pressure and temperature. *Earth Planet. Sci. Lett.* **349**, 15–25.

Williams-Jones A. E. and Heinrich C. A. (2005) 100th Anniversary special paper: vapor transport of metals and the formation of magmatic-hydrothermal ore deposits. *Econ. Geol.* **100**, 1287–1312.

Wu H. J., He Y. S., Bao L. E., Zhu C. W. and Li S. G. (2017) Mineral composition control on inter-mineral iron isotopic fractionation in granitoids. *Geochim. Cosmochim. Acta.* **198**, 208–217.

Xia Y., Li S. and Huang F. (2017) Iron and zinc isotope fractionation during magmatism in the continental crust: evidence from bimodal volcanic rocks from Hailar basin. *NE China. Geochim. Cosmochim. Acta* **213**, 35–46.

Xu L. J., He Y., Wang S. J., Wu H. and Li S. (2017) Iron isotope fractionation during crustal anatexis: Constraints from migmatites from the Dabie orogen, Central China. *Lithos* **284**, 171–179.

Zajacz Z., Halter W. E., Pettke T. and Guillong M. (2008) Determination of fluid/melt partition coefficients by LA-ICPMS analysis of co-existing fluid and silicate melt inclusions: controls on element partitioning. *Geochim. Cosmochim. Acta* **72**, 2169–2197.

Zambardi T., Lundstrom C. C., Li X. and McCurry M. (2014) Fe and Si isotope variations at Cedar Butte volcano; insight into magmatic differentiation. *Earth Planet. Sci. Lett.* **405**, 169–179.

Zhang Q. (2012) Could granitic magmas experience fractionation and evolution (in Chinese)? *Acta Petrol. Minerl.* **31**, 252–260 (in Chinese with English abstract).

Zhang Y., Xu Z., Zhu M. and Wang H. (2007) Silicate melt properties and volcanic eruptions. *Rev. Geophys.* **45**, RG4004. http://dx.doi.org/10.1029/2006RG000216.

Zhao G. and Cawood P. A. (2012) Precambrian geology of China. *Precambrian Res.* **222**, 13–54.

Associate editor: Fang-Zhen Teng